

FAPIS: A Few-shot Anchor-free Part-based Instance Segmenter

Khoi Nguyen and Sinisa Todorovic
Oregon State University
Corvallis, OR 97330, USA

{nguyenkh, sinisa}@oregonstate.edu

Abstract

This paper is about few-shot instance segmentation, where training and test image sets do not share the same object classes. We specify and evaluate a new few-shot anchor-free part-based instance segmenter (FAPIS). Our key novelty is in explicit modeling of latent object parts shared across training object classes, which is expected to facilitate our few-shot learning on new classes in testing. We specify a new anchor-free object detector aimed at scoring and regressing locations of foreground bounding boxes, as well as estimating relative importance of latent parts within each box. Also, we specify a new network for delineating and weighting latent parts for the final instance segmentation within every detected bounding box. Our evaluation on the benchmark COCO-20ⁱ dataset demonstrates that we significantly outperform the state of the art.

1. Introduction

This paper addresses the problem of few-shot instance segmentation. In training, we are given many pairs of support and query images showing instances of a target object class, and the goal is to produce a correct instance segmentation of the query given access to the ground-truth instance segmentation masks of the supports. In testing, we are given only one or a very few support images with their ground-truth instance segmentation masks, and a query image in which we are supposed to segment all instances of the target class. Importantly, the training and test image sets do not share the same object classes. Few-shot instance segmentation is a basic vision problem. It appears in many applications where providing manual segmentations of all object instances is prohibitively expensive. The key challenge is how to conduct a reliable training on small data.

Fig. 1 illustrates a common framework for few-shot instance segmentation that typically leverages Mask-RCNN [12, 43, 29]. First, the support and query images are input to a backbone CNN and feature pyramid network (FPN) [23] for computing the support’s and query’s feature maps.

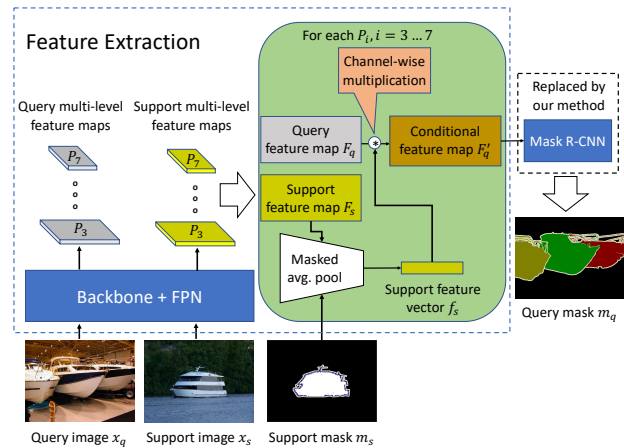


Figure 1. A common framework of prior work. The query and support image(s) are input to a backbone CNN with feature pyramid network (FPN) to extract the feature maps. The support’s features modulate the query’s features by channel-wise multiplication, resulting in the conditional query features, which are then input to Mask-RCNN for instance segmentation of the query. Our approach replaces Mask-RCNN with two new modules for anchor-free object detection, and part-based instance segmentation.

Second, for every feature map and every support’s segmentation mask, the masked average pooling computes the support’s feature vector. Third, the support’s feature vector is used to modulate the query’s feature maps through a channel-wise multiplication, resulting in the conditional query feature maps. Finally, the conditional query features are forwarded to the remaining modules of Mask-RCNN to produce instance segmentation of the query.

This framework has limitations. First, Mask-RCNN is anchor-based, and hence might overfit to particular sizes and aspect ratios of training objects, which do not characterize new classes in testing. Second, the Mask-RCNN learns feature prototypes [12] which are correlated with the feature map from the backbone in order to produce object segmentation. However, the prototypes typically capture global outlines of objects seen in training [12], and hence may not be suitable for segmenting new object classes with entirely

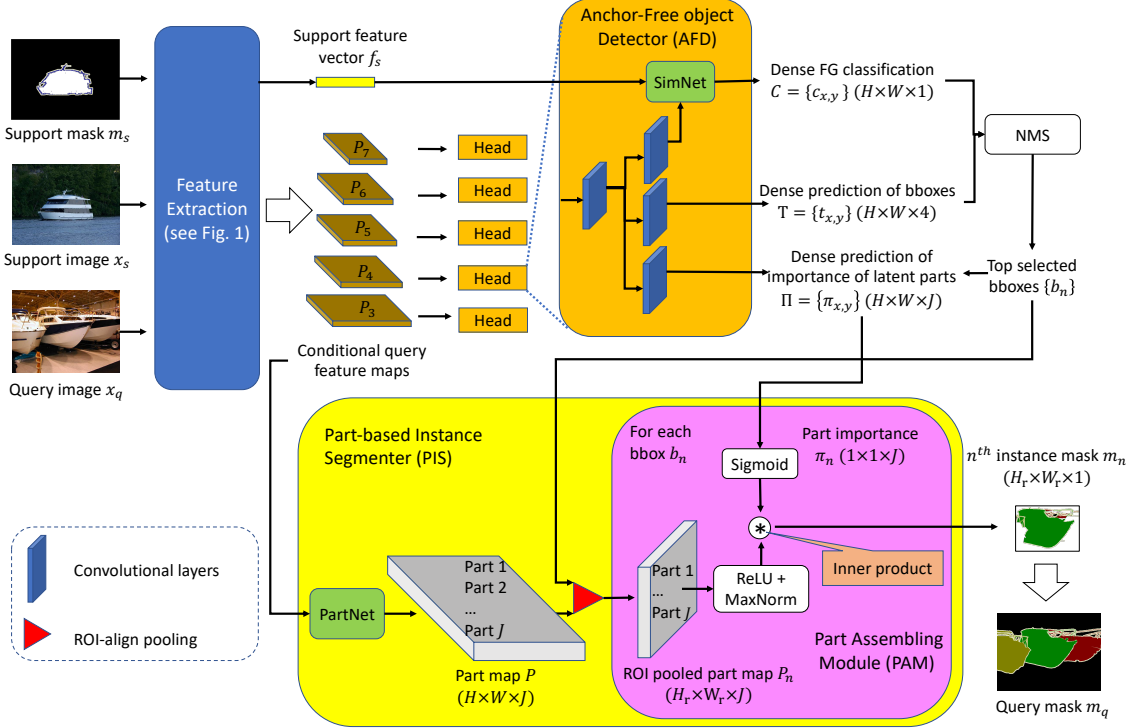


Figure 2. Our FAPIS uses the same feature maps as in Fig. 1, and extends prior work with two new modules: anchor-free object detector (AFD) and part-based instance segmenter (PIS). The AFD produces three types of dense predictions for every location (x, y) in the feature map: (a) Figure-ground (FG) classification score; (b) Location of the closest bounding box to (x, y) ; (c) Relative importance of the latent parts for segmentation of the bounding box closest to (x, y) . The PIS consists of the PartNet and Part Assembling Module (PAM). The PartNet predicts activation maps of the latent parts. After NMS selects the top scoring bounding boxes, for every box n , the PAM fuses the part-activation maps according to the predicted part importance for the box n , resulting in the instance segmentation m_n .

different shapes in testing.

To address these limitations, we propose FAPIS – a new **few-shot anchor-free part-based instance segmenter**, illustrated in Fig. 2. In a given query, FAPIS first detects bounding boxes of the target object class defined by the support image and its segmentation mask, and then segments each bounding box by localizing a universal set of latent object parts shared across all object classes seen in training.

Our key novelty is in explicit modeling of latent object parts, which are smaller object components but may not be meaningful (as there is no ground truth for parts). Unlike the prototypes of [12], our latent parts capture certain smaller components of objects estimated as important for segmentation. As parts may be shared by distinct objects, including new object classes of testing, we expect that accounting for parts will lead to a more reliable few-shot learning than the aforementioned common framework. We are not aware of prior work that learns latent parts for few-shot instance segmentation.

We make two contributions. First, we specify a new *anchor-free object detector* (AFD) that does not use a set of candidate bounding boxes with pre-defined sizes and as-

pect ratios, called anchors, and, as shown in [39], in this way mitigates over-fitting to a particular choice of anchors. The AFD (the orange box in Fig. 2) is aimed at three tasks at every location of the query’s feature map: dense scoring and regressing locations of foreground bounding boxes, as well as dense estimation of a relative importance of the latent parts for segmentation. While all of the latent parts are learned to be relevant for object segmentation, differences in sizes and shapes across instances will render some latent parts more important than some others for segmentation of each instance. Thus, the third head in the AFD estimates the part importance which varies across the predicted bounding boxes in the image, as desired. The AFD’s output is passed to the standard non-maximum suppression (NMS) for selecting top scoring bounding boxes.

Second, we specify a new *Part-based instance segmenter* (PIS). The PIS (the yellow box in Fig. 2) is aimed at localizing and integrating latent object parts to produce the final instance segmentation within every NMS-selected bounding box. The PIS consists of the PartNet and part assembling module (PAM). The PartNet predicts activation maps of the latent parts, called part maps, where large activations

strongly indicate the presence of the corresponding part in the image. Importantly, high activations of a certain latent part at image location (x, y) may not be important for segmentation of the object instance at (x, y) (e.g., when several latent parts overlap but do not “cover” the full spatial extent of the instance). Therefore, for every NMS-selected bounding box, these part maps are then integrated by the PAM so as to account for the predicted relative importance of the parts for that box. Finally, all instance segmentations form the output query segmentation mask.

Our evaluation on the COCO-20ⁱ dataset [29] demonstrates that we significantly outperform the state of the art.

In the following, Sec. 2 reviews prior work; Sec. 3 specifies our deep architecture; Sec. 4 presents our implementation details and experimental results; and Sec. 5 describes our concluding remarks.

2. Related Work

Few-shot semantic segmentation labels pixels in the query with target classes, each defined by K support examples [36, 32, 33, 6, 47, 38, 28, 14, 37, 46, 45, 44, 31, 41]. Our problem is arguably more challenging than few-shot semantic segmentation, since we need to additionally distinguish object instances of the same class.

Instance segmentation localizes instances of object classes seen in training, whereas we are supposed to segment instances of new classes. There are proposal-based and proposal-free approaches. The former [12, 22, 4, 27, 1] first detects object bounding boxes, and then segments foreground within every box. The latter [16, 17, 2, 8] typically starts from a semantic segmentation, and then leverages certain visual cues (e.g., object center, or Watershed energy) to cluster pixels of the same semantic class into instances.

Our FAPIS and YOLACT [1] are similar in that they both predict activation maps of certain object features, and at each location in the image they fuse these activation maps by weighting their relative importance for segmentation. However, since YOLACT is not aimed at the few-shot setting, there are a number of significant differences. First, our FAPIS models latent object parts, whereas YOLACT models object prototypes representing global outlines of groups of similar object shapes. While the latter has been argued as suitable for instance segmentation, our experiments demonstrate that the prototypes learned on training examples poorly represent new, differently shaped object classes in testing for few-shot instance segmentation. As our latent parts may be components of the new object classes, they are likely to better represent new objects than the global shapes of prototypes. Second, YOLACT is standard anchor-based detector, whereas our AFD object detector is anchor-free producing dense predictions of bounding boxes. Our approach is more suitable for few-shot instance segmentation, as pre-defined anchors in training may not represent well

the sizes and aspect ratios of new objects in testing.

Few-shot instance segmentation approaches usually adapt methods for instance segmentation (e.g., Mask-RCNN [12]) to the few-shot setting [29, 43, 7] (see Fig. 1). Our main differences are in replacing the Mask-RCNN with our AFD and PID for modeling latent object parts and segmenting every detected instance by localizing and assembling latent parts relevant for that instance.

Anchor-free Object Detection [39, 48, 19] predicts bounding boxes for all pixels in the feature map. This is opposite to anchor-based approaches [34, 24] where a set of bounding boxes with pre-defined sizes and aspect ratios are classified as presence or absence. Our AFD follows the FCOS approach [39], where at each location (x, y) distances to the top, bottom, left, right sides of the closest bounding box are predicted by regression. We extend FCOS with SimNet to more reliably score bounding boxes, and thus reduce the number of false positives.

Part-based segmentation. While the literature abounds with approaches that use parts for image classification and object detection, there is relatively scant work on part-based segmentation. In [40, 10] the deformable part model [9] is used for semantic segmentation, and in [26] reasoning about “left”, “right”, “bottom” and “top” parts of the foreground object is shown to help instance segmentation. Recent work [21, 11] addresses the problem of human (one class) segmentation, not our multi-class segmentation problem. We are not aware of prior work that learns latent parts for few-shot instance segmentation.

3. Our Approach

3.1. Problem Statement

In training, we are given many pairs of support and query images showing the same target class from the class set \mathcal{C}_1 , along with their pixel-wise annotations of every instance of the target class. In testing, we are given K support images, $\{x_s\}$, and their K instance segmentation masks $\{m_s\}$ that define a target class sampled from the class set \mathcal{C}_2 , where $\mathcal{C}_1 \cap \mathcal{C}_2 = \emptyset$. Given a test query, x_q , showing the same target class as the test supports, our goal is to segment all foreground instances in x_q , i.e., estimate the query instance segmentation mask m_q . This problem is called **1-way K -shot instance segmentation**. In this paper, we consider $K = 1$ and $K = 5$, i.e., test settings with a very few supports. It is worth noting that we can easily extend the 1-way K -shot to N -way K -shot by running N support classes on the same query, since every class can be independently detected. However, the N -way K -shot problem is beyond the scope of this paper.

3.2. Multi-level Feature Extraction

As shown in Fig. 1, FAPIS first extracts multi-level feature maps at different resolutions from x_s and x_q using a backbone CNN with feature pyramid network (FPN), as in [23]. For each level $i = 3, 4, \dots, 7$, the support feature map $F_{s,i}$ is masked-average pooled within a down-sampled version of the support mask m_s to obtain the support feature vector $f_{s,i}$. Then, for each level i , $f_{s,i}$ is used to modulate the corresponding query feature map $F_{q,i}$. Specifically, $f_{s,i}$ and $F_{q,i}$ are multiplied channel-wise. This gives the conditional query feature map $F'_{q,i}$. The channel-wise multiplication increases (or decreases) activations in the query's $F'_{q,i}$ when the corresponding support's activations are high (or low). In this way, the channel features that are relevant for the target class are augmented, and irrelevant features are suppressed to facilitate instance segmentation.

3.3. The Anchor-free Object Detector

For each conditional query feature map $F'_{q,i}$, $i = 3, 4, \dots, 7$, the AFD scores and regresses locations of foreground bounding boxes. Below, for simplicity, we drop the notation i for the feature level, noting that the same processing is done for each level i . The workflow of the AFD is illustrated in the orange box in Fig. 2.

For every location (x, y) in F'_q with height and width $H \times W$, the AFD predicts:

1. Figure-ground (FG) classification scores $C = \{c_{x,y}\} \in [0, 1]^{H \times W}$ using the SimNet and Classification Head;
2. Regressions $T = \{t_{x,y}\} \in \mathbb{R}_+^{H \times W \times 4}$ of top, bottom, left, right distances from (x, y) to the closest box.
3. Relative importance of the J latent parts for instance segmentation of the bounding box predicted at (x, y) , $\Pi = \{\pi_{x,y}\} \in \mathbb{R}^{H \times W \times J}$.

SimNet and Classification Head. Prior work [43, 29], uses the support feature vector to modulate the query feature map by channel-wise multiplication, and thus detect target objects. However, in our experiments, we have observed that this method results in a high false-positive rate. To address this issue, we specify the SimNet which consists of a block of fully connected layers followed by a single convolutional layer. The first block takes as input f_s and predicts weights of the top convolutional layer. This is suitable for addressing new classes in testing. Then, the top convolutional layer takes as input F'_q and the resulting feature maps are passed to the FG head for predicting the FG classification scores C at every location (x, y) . In this way, the SimNet learns how to more effectively modulate F'_q , extending the channel-wise multiplication in [43, 29].

For training the FG head, we use the focal loss [24]:

$$L_c = \frac{-1}{H \times W} \sum_{x,y} \alpha'_{x,y} (1 - c'_{x,y})^\gamma \log(c'_{x,y}), \quad (1)$$

where $c'_{x,y} = c_{x,y}^* c_{x,y} + (1 - c_{x,y}^*) (1 - c_{x,y})$, $c_{x,y}^* \in \{0, 1\}$ is the ground-truth classification score at (x, y) ; $\alpha'_{x,y} = c_{x,y}^* \alpha + (1 - c_{x,y}^*) (1 - \alpha)$, $\alpha \in [0, 1]$ is a balance factor of classes, and $\gamma \in [0, 5]$ is a focusing parameter to smoothly adjust the rate at which easy examples are down-weighted.

Bounding Box Regression. For training the box regression head, we use the general intersection-over-union (GIoU) loss [35]:

$$L_b = \frac{1}{N_{pos}} \sum_{x,y} \mathbb{1}(c_{x,y}^* = 1) \cdot \text{GIoU}(t_{x,y}, t_{x,y}^*), \quad (2)$$

where $t_{x,y}^* \in \mathbb{R}_+^4$ is a vector of the ground-truth top, bottom, left, right box distances from (x, y) ; $\mathbb{1}(\cdot)$ is the indicator function having value 1 if (x, y) belongs to the ground-truth box and 0 otherwise; and $N_{pos} = \sum_{x,y} \mathbb{1}(c_{x,y}^* = 1)$ is the number of locations in the feature map that belong to the foreground.

Part-Importance Prediction Head. For every location (x, y) in F'_q , this head predicts the relative importance of the latent parts $\Pi = \{\pi_{x,y}\} \in \mathbb{R}^{H \times W \times J}$. This part-importance prediction seeks to capture the varying dependencies among the latent parts when jointly used to estimate a segmentation mask of the bounding box predicted for every (x, y) . Note that we are not in a position to specify an explicit loss for training this head, because the parts are latent, and not annotated in our training set. Importantly, we do get to train this head by backpropagating the instance segmentation loss, as described in Sec. 3.4.

The AFD's predictions are forwarded to the standard NMS to select the top scoring $n = 1, \dots, N$ bounding boxes at all feature-pyramid levels.

3.4. The Part-based Instance Segmenter

The PIS is illustrated in the yellow box in Fig. 2. The PIS consists of the PartNet and the PAM.

The PartNet takes as input the largest conditional query feature map – specifically, $F'_{q,3}$ – and predicts activation maps of the J latent parts, or part maps for short, $P \in \mathbb{R}^{H \times W \times J}$. J is a hyper-parameter that we experimentally set to an optimal value. High activations in P for a particular latent part at location (x, y) strongly indicate that part's presence at (x, y) . For every bounding box $n = 1, \dots, N$ selected by the NMS, we conduct region-of-interest (ROI) aligned pooling of P to derive the J ROI-aligned pooled part maps $P_n \in \mathbb{R}^{H_r \times W_r \times J}$, where H_r and W_r are the reference height and width ensuring that the pooled features of the N bounding boxes have the same reference dimension. The PartNet is learned by backpropagation of the instance segmentation loss through the PAM module, since the latent parts are not annotated and we cannot define an explicit loss for training the PartNet.

A strongly indicated presence of a certain latent part at location (x, y) in P_n may not be important for segmentation

of the object instance in the bounding box n (e.g., when this information is redundant as many other latent parts may also have a high activation at (x, y) in P_n). For each location, we obtain a triplet of classification scores, bounding box and part importance π_n . Therefore, for every bounding box $n = 1, \dots, N$, the following PAM module takes as input both the pooled part maps $P_n \in \mathbb{R}^{H_r \times W_r \times J}$ and the estimated part importance $\pi_n \in \mathbb{R}^J$ for segmentation of instance n .

The PAM computes the segmentation mask of every bounding box $n = 1, \dots, N$, $m_n \in [0, 1]^{H_r \times W_r}$, as

$$m_n = P_n^+ \otimes \sigma(\pi_n), \quad P_n^+ = \text{MaxNorm}(\text{ReLU}(P_n)), \quad (3)$$

where $\text{MaxNorm}(A) = \frac{A}{\max_{x,y} A_{x,y}}$ for an activation map A , \otimes denotes a inner product, and σ is the sigmoid function. Note that \otimes in (3) requires the tensor P_n^+ be rectified to a matrix of size $(H_r W_r) \times J$. Thus, the operator \otimes serves to fuse the part maps by their respective importance for instance segmentation.

The MaxNorm-ReLU composite function and the sigmoid in (3) make the part maps and their importance non-negative with values in $[0, 1]$. This design choice is inspired by the well-known *non-negative matrix factorization* (NMF) [20], so that if the instance segmentation matrix m_n were available, the expression in (3) would amount to the NMF of m_n into the non-negative P_n^+ and $\sigma(\pi_n)$. This design choice is conveniently used to regularize learning of the PartNet and the AFD’s head for predicting the part importance. Specifically, in learning, we maximize similarity between the predicted P_n^+ and the NMF’s bases computed for the ground-truth instance segmentation masks $\{m_n^* : n = 1, \dots, D\}$, where D is the total number of instances in the training set. This NMF-based regularization in learning enforces that our P_n^+ is *sparse*, justifying our interpretation that P_n^+ represents the smaller latent parts of object instances.

Segmentation loss and NMF-based regularization. The prediction m_n , given by (3), incurs the following segmentation loss L_s with respect to the ground-truth instance segmentation mask m_n^* :

$$L_s = \frac{1}{N} \sum_{n=1}^N l_{dice}(m_n, m_n^*), \quad (4)$$

$$l_{dice}(A, B) = 1 - \frac{2 \sum_{x,y} A_{x,y} \cdot B_{x,y}}{\sum_{x,y} A_{x,y}^2 + \sum_{x,y} B_{x,y}^2},$$

where l_{dice} is the dice loss [30] between maps A and B .

L_s is backpropagated through the PAM to the PartNet and AFD for improving the predictions P and Π such that L_s is minimized. We regularize this learning by using the NMF of the ground-truth instance segmentation masks as follows. All ground-truth segmentations of all object classes in the training dataset $\{m_n^* : n = 1, \dots, D\}$ are first re-sized and stacked into a large $(H_r W_r) \times D$ matrix M^* .

Then, we apply the NMF as $M^* \approx P^* U$, where P^* is the non-negative basis matrix with size $(H_r W_r) \times J$, and U is the non-negative weight matrix with size $J \times D$. The product $P^* U$ is a low-rank approximation of M^* . Due to the non-negative constraint, P^* is forced to be sparse. Fig. 3 shows the NMF’s bases in P^* that we computed on the ground-truth masks $\{m_n^*\}$ of the COCO-20ⁱ dataset [29]. Hence, P^* is interpreted as storing parts of all training object classes in M^* . Conveniently, the NMF, i.e., P^* , can be pre-computed before learning.

We use P^* to regularize our learning of the PartNet such that it produces part maps P_n^+ that are similar to P^* . Note that the J latent parts in P_n^+ may be differently indexed from the NMF’s J bases stored in P^* . Therefore, we employ the Hungarian algorithm [18] to identify the one-to-one correspondence between the latent parts $P_{n,j}^+$ and the bases $P_{j'}^*$, $j' = \text{Hungarian}(j)$, $j = 1, \dots, J$, based on their intersection-over-union (IoU) score. With this correspondence, we specify the NMF regularization loss as

$$L_{\text{NMF}} = \frac{1}{N} \sum_{n=1}^N \sum_{j=1}^J l_{dice}(P_{n,j}^+, P_{j'}^*), \quad j' = \text{Hungarian}(j). \quad (5)$$

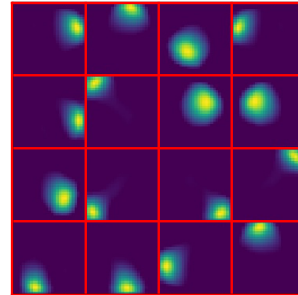


Figure 3. Visualization of 16 NMF parts estimated from the size-normalized ground-truth instance masks in COCO-20ⁱ [29].

The total loss for training our FAPIS is specified as

$$L = \lambda_1 L_c + \lambda_2 L_b + \lambda_3 L_s + \lambda_4 L_{\text{NMF}} \quad (6)$$

where the λ ’s are positive coefficients, specified in Sec. 4.1.

4. Experiments

Dataset & Metrics: For evaluation, we conduct the standard 4-fold cross-validation on the benchmark COCO-20ⁱ dataset [29]. In each fold $i = 0, \dots, 3$, we sample 20 test classes from the 80 object classes in MSCOCO [25], and use the remaining 60 classes for training. For each COCO-20ⁱ, we randomly sample five separate test sets, and report the average results as well as their standard deviations, as in [29]. We follow the standard testing protocol for 1-way K -shot instance segmentation [29]. Our training uses $K = 1$

support image, while in testing we consider two settings with $K = 1$ and $K = 5$ support images. For each test query, K support images are randomly sampled from the remaining test images showing the same test class as the query. We use the evaluation tool provided by the COCO dataset to compute the following metrics: mAP50 of both segmentation and detection is computed at a single intersection-over-union (IoU) threshold of 50% between our prediction and ground truth; mAR10 is average recall given 10 detections per image. Our results of other metrics for each fold can be found in the supplementary material.

4.1. Implementation Details

Our backbone CNN is ResNet-50 [13] and the FPN of [23], as in prior work. FAPIS is implemented using the mmdetection toolbox [3]. We empirically find that using the P3 to P5 feature map levels gives the best results. The FG scoring and part-importance prediction share the first two convolutional layers with GroupNorm [42] and ReLU activation in between, but use two separate heads for binary class and part-importance predictions. We strictly follow the design of classification head and box regression head of FCOS [39]. SimNet has a block of four fully connected layers with BatchNorm [15] and ReLU in between each layer, followed by a top convolutional layer, where the block predicts the weights of the top layer. The PartNet consists of 5 convolutional layers with GroupNorm and ReLU, and an Upsampling layer to upscale the resolution by two in the middle of layer 3 and 4, following the design of mask head of Mask-RCNN [12]. For learning, we use SGD with momentum [5] with the learning rate of $1e^{-3}$. The number of training epochs is 12, which is similar to the setting of 1x in Mask-RCNN. The mini-batch size is 16. The query images are resized to 800×1333 pixels. The support images and masks are cropped around the ground-truth bounding boxes and re-sized to 128×128 pixels. We set $H_r = W_r = 32$, $\alpha = 0.25$ and $\gamma = 2$ in (1), and $\lambda_1 = \lambda_2 = \lambda_3 = 1$, $\lambda_4 = 0.1$ in (6).

4.2. Ablation Study

Ablations and sensitivity to input parameters are evaluated for the setting $K = 1$.

Analysis of the number of parts. Tab. 1 reports how the number of latent parts J affects our results. We vary J while keeping other hyper-parameters unchanged. From Tab. 1, $J = 16$ gives the best performance. When J is small, FAPIS cannot reliably capture object variations, and when J approaches the number of classes considered in training, the PartNet tends to predict shape prototypes as in YOLACT [1], instead of parts. Therefore, we use $J = 16$ for all other evaluations.

Analysis of the predicted part importance. Tab. 2 shows a percentage of the latent parts whose predicted im-

# parts	1	2	4	8	16	32	64
mAP50	16.3	17.2	17.9	18.4	18.8	18.5	18.0

Table 1. mAP50 for segmentation of FAPIS on COCO-20⁰ for different numbers of the latent parts J used.

θ	0.1	0.3	0.5	0.7	0.9
% parts with $\sigma(\pi) > \theta$	0.32	0.29	0.26	0.21	0.09

Table 2. The predicted importance of most latent parts is on average lower than a threshold $\theta \in (0, 1)$, so instance segmentation is formed from only a few important parts.

Ablations	Object detection		Instance segm	
	mAP50	mAR10	mAP50	mAR10
FIS	18.4	25.0	16.4	21.3
FAIS	20.9	28.1	18.0	22.5
FAIS-SimNet	20.2	26.9	17.4	22.0
FAIS-CWM	16.5	24.3	15.4	20.5
FPIS	18.4	25.0	17.4	22.4
FAPIS- L_{NMF}	20.5	27.5	18.4	22.7
FAPIS	20.9	28.1	18.8	23.3

Table 3. mAP50 and mAR10 of one-shot object detection and instance segmentation on COCO-20⁰ for different variants of FAPIS. The PIS is used only for instance segmentation, so the variants FIS and FPIS have lower mAP50 for object detection. The AFD is used for both instance detection and segmentation, and thus FAIS and FAPIS have higher mAP50 for both object detection and instance segmentation than FIS and FPIS. The AFD without SimNet decreases its discriminative power so FAIS-SimNet has lower mAP50 for object detection than FAIS. When the channel-wise multiplication (CWM) is replaced with SimNet alone, performance of FAIS significantly decreases, and becomes even lower than that of FIS. This shows that SimNet does not replace but extends CWM. FAPIS- L_{NMF} has lower mAP50 for instance segmentation than FAPIS.

portance for segmentation is higher than a threshold $\theta \in (0, 1)$. As can be seen, for a given object instance, most latent parts are usually estimated as irrelevant. That is, the PAM essentially uses only a few most important latent parts to form the instance segmentation mask.

Ablations of FAPIS. Tab. 3 demonstrates how the AFD and PIS affect performance of the following six ablations:

- FIS: AFD is replaced with the region proposal network (RPN) [34] for anchor-based detection; and PIS is replaced with the standard mask-head of Mask-RCNN.
- FAIS: PIS replaced with mask-head of Mask-RCNN.
- FAIS-SimNet: FAIS without SimNet, and FG scores are predicted as in [39] (see Fig. 1).
- FAIS-CWM: FAIS without channel-wise multiplication (CWM).
- FPIS: AFD is replaced with RPN [34]

- FAPIS- L_{NMF} : FAPIS trained without the regularization loss L_{NMF} .
- FAPIS: our approach depicted in Fig. 2

The top three variants test our contributions related to anchor-free detection, and the last three test our contributions related to modeling the latent parts.

From Tab. 3, our AFD in FAIS improves performance by 1.6% on mAP50 over FIS that uses the anchor-based detector. However, removing the SimNet from the AFD in FAIS-SimNet decreases performance, justifying our SimNet as a better way to predict FG scores than in [43, 29]. The PIS in FPIS gives a performance gain of 1% on mAP50 in instance segmentation over FIS. Our performance decreases when FAPIS is trained without the NMF regularization in FAPIS- L_{NMF} . FAPIS gives the best performance in comparison with the strong baselines.

Note that we cannot directly evaluate our part detection, since we do not have ground-truth annotations of parts.

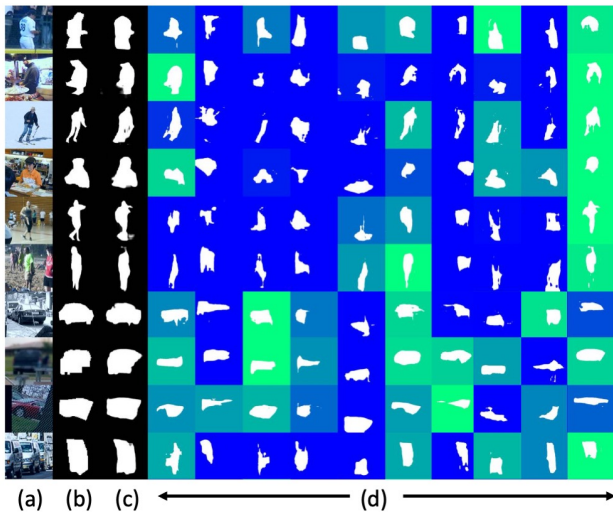


Figure 4. Visualization of the most important 10 latent parts out of 16 predicted for example instances of the “human” and “car” classes from the COCO-20⁰ validation dataset. From left to right: (a) input image, (b) GT segmentation, (c) predicted segmentation, (d) 10 most relevant parts. The predicted importance of the parts is color-coded from blue (smallest) to green (largest).

4.3. Comparison with prior work

FAPIS is compared with Meta-RCNN [43], Siamese Mask-RCNN [29] and YOLACT [1]. Meta-RCNN and Siamese Mask-RCNN use the same anchor-based framework, but differ in that Meta-RCNN performs the feature correlation after the RPN, whereas Siamese Mask-RCNN does this before the RPN. YOLACT is another anchor-based instance segmentor based on RetinaNet [24], which learns to predict object shapes instead of object parts, and we adapt it to few-shot instance segmentation by changing

its feature extraction module as in Fig. 1.

Note that the results of Siamese Mask-RCNN in [29] are reported for evaluation where the support images do not provide ground-truth segmentation masks, but only bounding boxes. Therefore, for fairness, we evaluate Siamese Mask-RCNN (without any changes to their public code) on the same input as for Meta-RCNN, YOLACT, and FAPIS—i.e., when the support images provide ground-truth segmentation masks of object instances. In addition, in [43], the results of Meta-RCNN are reported for a different version of COCO. Therefore, we evaluate Meta-RCNN (without any changes to their public code) on our test sets.

Tab. 4 reports one-shot and five-shot object detection results, and Tab. 5 shows one-shot and five-shot instance segmentation results. From these tables, Siamese Mask-RCNN performs slightly better than Meta-RCNN, since the feature correlation happens before the RPN, enabling the RPN to better adapt its bounding box proposals to the target class. Our FAPIS outperforms YOLACT by 2% for one-shot and five-shot instance segmentation. This demonstrates advantages of using latent parts and their layouts for assembling object shapes in our approach over the YOLACT’s prototypes in few-shot instance segmentation.

Our gains in performance are significant in the context of previous performance improvements reported by prior work, where gains were only by about 0.6% by [29] vs [43], by 0.1% by [29] vs [1], by 0.5 % [1] vs [43]. We improve by 1.8% and 2.0% over [29] on one-shot and five-shot instance segmentation, respectively.

4.4. Qualitative Evaluation

Fig. 9 visualizes the most important 10 of 16 latent parts and their relative importance for a few example instances of the “human” and “car” classes from the COCO-20⁰ validation set. The figure shows that the predicted latent parts are smaller components of the objects, and that some parts may be assigned a meaningful interpretation. Our visualization of the latent parts for other classes can be found in the supplementary material.

A few representative success and failure results on COCO-20⁰ are illustrated in Fig. 5, and others are included in the supplementary material.

5. Conclusion

We have specified a new few-shot anchor-free part-based instance segmenter (FAPIS) that predicts latent object parts for instance segmentation, where part annotations are not available in training. FAPIS uses our new anchor-free object detector (AFD), PartNet for localizing the latent parts, and part assembly module for fusing the part activation maps by their predicted importance into a segmentation of every detected instance. We have regularized learning such that the identified latent parts and similar to the sparse bases of the

# shots	Method	COCO-20 ⁰	COCO-20 ¹	COCO-20 ²	COCO-20 ³	mean
K=1	Meta-RCNN [43]	17.7 ± 0.7	19.2 ± 0.6	17.7 ± 0.3	21.1 ± 0.4	18.9
	Siamese M-RCNN [29]	18.3 ± 0.8	19.5 ± 0.7	18.0 ± 0.4	21.5 ± 0.6	19.3
	YOACT [1]	18.0 ± 0.5	18.8 ± 0.5	17.8 ± 0.6	21.2 ± 0.7	19.0
	FAPIS	20.9 ± 0.4	20.4 ± 0.1	20.0 ± 0.6	23.4 ± 0.5	21.2
K=5	Meta-RCNN [43]	19.1 ± 0.4	21.2 ± 0.2	19.6 ± 0.5	24.0 ± 0.2	21.0
	Siamese M-RCNN [29]	20.0 ± 0.4	21.6 ± 0.3	20.2 ± 0.4	24.1 ± 0.3	21.5
	YOACT [1]	20.8 ± 0.4	21.1 ± 0.2	20.2 ± 0.5	24.8 ± 0.2	21.7
	FAPIS	22.6 ± 0.3	22.8 ± 0.0	22.6 ± 0.6	26.4 ± 0.2	23.6

Table 4. mAP50 with standard deviation of one-shot and five-shot **object detection** on COCO-20ⁱ. The best results are in bold.

# shots	Method	COCO-20 ⁰	COCO-20 ¹	COCO-20 ²	COCO-20 ³	mean
K=1	Meta-RCNN [43]	16.0 ± 0.6	16.1 ± 0.5	15.8 ± 0.3	18.6 ± 0.4	16.6
	Siamese M-RCNN [29]	16.6 ± 0.8	16.6 ± 0.6	16.3 ± 0.7	19.3 ± 0.6	17.2
	YOACT [1]	16.8 ± 0.6	16.5 ± 0.5	16.1 ± 0.4	19.0 ± 0.6	17.1
	FAPIS	18.8 ± 0.3	17.7 ± 0.1	18.2 ± 0.7	21.4 ± 0.4	19.0
K=5	Meta-RCNN [43]	17.4 ± 0.3	17.8 ± 0.2	17.7 ± 0.7	21.3 ± 0.2	18.6
	Siamese M-RCNN [29]	17.5 ± 0.4	18.5 ± 0.1	18.2 ± 1.0	22.4 ± 0.2	19.2
	YOACT [1]	17.6 ± 0.2	18.4 ± 0.2	17.9 ± 0.6	21.8 ± 0.3	18.9
	FAPIS	20.2 ± 0.2	20.0 ± 0.1	20.4 ± 0.7	24.3 ± 0.2	21.2

Table 5. mAP50 with standard deviation of one-shot and five-shot **instance segmentation** on COCO-20ⁱ. The best results are in bold.

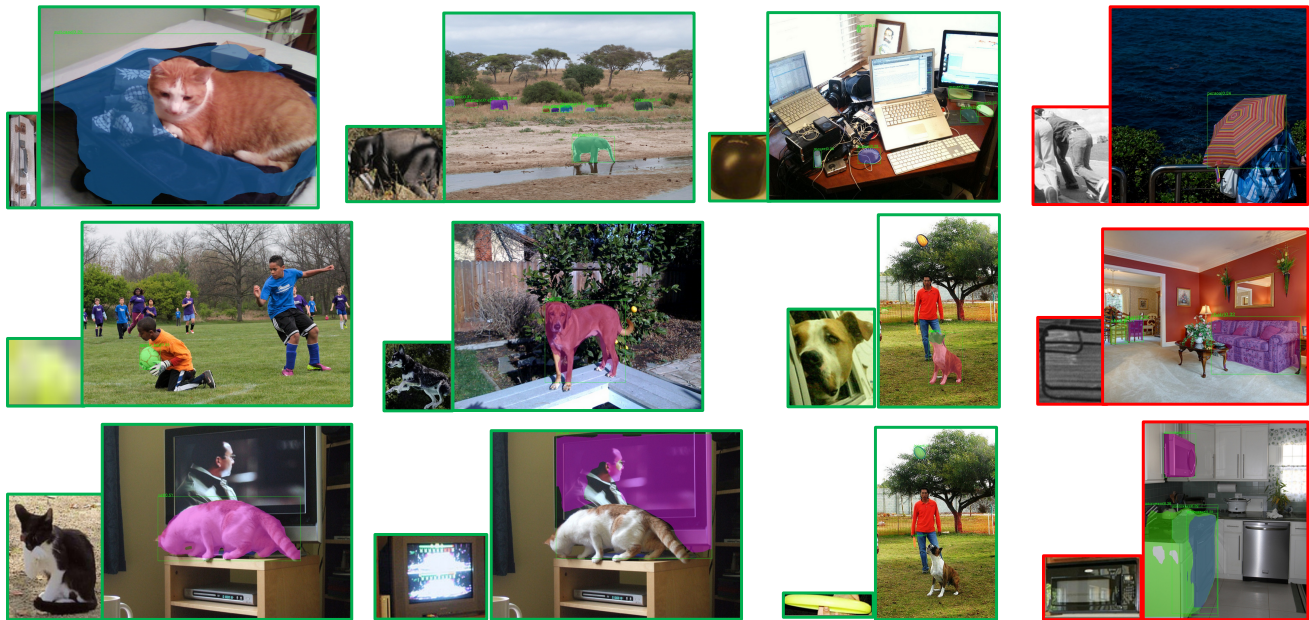


Figure 5. Our one-shot instance segmentation on COCO-20⁰. For each pair of images, the support is the smaller and the query is the larger image. Results for the segmentation and bounding-box detection of each instance are marked with distinct colors in the query. The green border indicates success, and the red border marks failure. FAPIS typically fails when instances in the support image are very different in appearance, shape, or 3D pose from instances in the query. Best viewed in color.

non-negative matrix factorization of the ground-truth segmentation masks. Our evaluation on the benchmark COCO-20ⁱ dataset demonstrates that: we significantly outperform the state of the art; our prediction of latent parts gives better performance than using the YOACT’s prototypes or using the standard mask-head of Mask-RCNN; and our anchor-

free AFD improves performance over the common anchor-based bounding-box prediction.

Acknowledgement. This work was supported in part by DARPA XAI Award N66001-17-2-4029 and DARPA MCS Award N66001-19-2-4035.

References

- [1] Daniel Bolya, Chong Zhou, Fanyi Xiao, and Yong Jae Lee. Yolact: real-time instance segmentation. In *Proceedings of the IEEE International Conference on Computer Vision*, pages 9157–9166, 2019. 3, 6, 7, 8
- [2] Siddhartha Chandra, Nicolas Usunier, and Iasonas Kokkinos. Dense and low-rank gaussian crfs using deep embeddings. In *Proceedings of the IEEE International Conference on Computer Vision*, pages 5103–5112, 2017. 3
- [3] Kai Chen, Jiaqi Wang, Jiangmiao Pang, Yuhang Cao, Yu Xiong, Xiaoxiao Li, Shuyang Sun, Wansen Feng, Ziwei Liu, Jiarui Xu, et al. Mmdetection: Open mmlab detection toolbox and benchmark. *arXiv preprint arXiv:1906.07155*, 2019. 6
- [4] Liang-Chieh Chen, Alexander Hermans, George Papandreou, Florian Schroff, Peng Wang, and Hartwig Adam. Masklab: Instance segmentation by refining object detection with semantic and direction features. In *Proceedings of the IEEE Conference on Computer Vision and Pattern Recognition*, pages 4013–4022, 2018. 3
- [5] Corinna Cortes and Vladimir Vapnik. Support-vector networks. *Machine learning*, 20(3):273–297, 1995. 6
- [6] Nanqing Dong and Eric P Xing. Few-shot semantic segmentation with prototype learning. In *BMVC*, volume 3, page 4, 2018. 3
- [7] Zhibo Fan, Jin-Gang Yu, Zhihao Liang, Jiarong Ou, Changxin Gao, Gui-Song Xia, and Yuanqing Li. Fgn: Fully guided network for few-shot instance segmentation. In *Proceedings of the IEEE/CVF Conference on Computer Vision and Pattern Recognition*, pages 9172–9181, 2020. 3
- [8] Alireza Fathi, Zbigniew Wojna, Vivek Rathod, Peng Wang, Hyun Oh Song, Sergio Guadarrama, and Kevin P Murphy. Semantic instance segmentation via deep metric learning. *arXiv preprint arXiv:1703.10277*, 2017. 3
- [9] Pedro F. Felzenszwalb, Ross B. Girshick, David McAllester, and Deva Ramanan. Object detection with discriminatively trained part-based models. *IEEE Trans. Pattern Anal. Mach. Intell.*, 32(9):1627–1645, 2010. 3
- [10] Ross Girshick, Jeff Donahue, Trevor Darrell, and Jitendra Malik. Rich feature hierarchies for accurate object detection and semantic segmentation. In *Proceedings of the IEEE conference on computer vision and pattern recognition*, pages 580–587, 2014. 3
- [11] Ke Gong, Xiaodan Liang, Yicheng Li, Yimin Chen, Ming Yang, and Liang Lin. Instance-level human parsing via part grouping network. In *Proceedings of the European Conference on Computer Vision (ECCV)*, pages 770–785, 2018. 3
- [12] Kaiming He, Georgia Gkioxari, Piotr Dollár, and Ross Girshick. Mask r-cnn. In *Proceedings of the IEEE international conference on computer vision*, pages 2961–2969, 2017. 1, 2, 3, 6
- [13] Kaiming He, Xiangyu Zhang, Shaoqing Ren, and Jian Sun. Deep residual learning for image recognition. In *The IEEE Conference on Computer Vision and Pattern Recognition (CVPR)*, June 2016. 6
- [14] Tao Hu, Pengwan Yang, Chiliang Zhang, Gang Yu, Yadong Mu, and Cees GM Snoek. Attention-based multi-context guiding for few-shot semantic segmentation. In *Proceedings of the AAAI Conference on Artificial Intelligence*, volume 33, pages 8441–8448, 2019. 3
- [15] Sergey Ioffe and Christian Szegedy. Batch normalization: Accelerating deep network training by reducing internal covariate shift. *arXiv preprint arXiv:1502.03167*, 2015. 6
- [16] Alexander Kirillov, Evgeny Levinkov, Bjoern Andres, Bogdan Savchynskyy, and Carsten Rother. Instancecut: from edges to instances with multicut. In *Proceedings of the IEEE Conference on Computer Vision and Pattern Recognition*, pages 5008–5017, 2017. 3
- [17] Shu Kong and Charless C Fowlkes. Recurrent pixel embedding for instance grouping. In *Proceedings of the IEEE Conference on Computer Vision and Pattern Recognition*, pages 9018–9028, 2018. 3
- [18] Harold W Kuhn. The hungarian method for the assignment problem. *Naval research logistics quarterly*, 2(1-2):83–97, 1955. 5
- [19] Hei Law and Jia Deng. Cornernet: Detecting objects as paired keypoints. In *Proceedings of the European Conference on Computer Vision (ECCV)*, pages 734–750, 2018. 3
- [20] Daniel D Lee and H Sebastian Seung. Learning the parts of objects by non-negative matrix factorization. *Nature*, 401(6755):788–791, 1999. 5
- [21] Qizhu Li, Anurag Arnab, and Philip HS Torr. Holistic, instance-level human parsing. *arXiv preprint arXiv:1709.03612*, 2017. 3
- [22] Yi Li, Haozhi Qi, Jifeng Dai, Xiangyang Ji, and Yichen Wei. Fully convolutional instance-aware semantic segmentation. In *Proceedings of the IEEE Conference on Computer Vision and Pattern Recognition*, pages 2359–2367, 2017. 3
- [23] Tsung-Yi Lin, Piotr Dollár, Ross Girshick, Kaiming He, Bharath Hariharan, and Serge Belongie. Feature pyramid networks for object detection. In *Proceedings of the IEEE conference on computer vision and pattern recognition*, pages 2117–2125, 2017. 1, 4, 6
- [24] Tsung-Yi Lin, Priya Goyal, Ross Girshick, Kaiming He, and Piotr Dollár. Focal loss for dense object detection. In *Proceedings of the IEEE international conference on computer vision*, pages 2980–2988, 2017. 3, 4, 7
- [25] Tsung-Yi Lin, Michael Maire, Serge Belongie, Lubomir Bourdev, Ross Girshick, James Hays, Pietro Perona, Deva Ramanan, C. Lawrence Zitnick, and Piotr Dollár. Microsoft coco: Common objects in context. In *European conference on computer vision (ECCV)*, June 2016. 5
- [26] Shu Liu, Jiaya Jia, Sanja Fidler, and Raquel Urtasun. Sgn: Sequential grouping networks for instance segmentation. In *Proceedings of the IEEE International Conference on Computer Vision*, pages 3496–3504, 2017. 3
- [27] Shu Liu, Lu Qi, Haifang Qin, Jianping Shi, and Jiaya Jia. Path aggregation network for instance segmentation. In *Proceedings of IEEE Conference on Computer Vision and Pattern Recognition (CVPR)*, 2018. 3
- [28] Jonathan Long, Evan Shelhamer, and Trevor Darrell. Fully convolutional networks for semantic segmentation. In *Proceedings of the IEEE conference on computer vision and pattern recognition*, pages 3431–3440, 2015. 3

- [29] Claudio Michaelis, Ivan Ustyuzhaninov, Matthias Bethge, and Alexander S Ecker. One-shot instance segmentation. *arXiv preprint arXiv:1811.11507*, 2018. 1, 3, 4, 5, 7, 8
- [30] Fausto Milletari, Nassir Navab, and Seyed-Ahmad Ahmadi. V-net: Fully convolutional neural networks for volumetric medical image segmentation. In *2016 fourth international conference on 3D vision (3DV)*, pages 565–571. IEEE, 2016. 5
- [31] Khoi Nguyen and Sinisa Todorovic. Feature weighting and boosting for few-shot segmentation. In *Proceedings of the IEEE International Conference on Computer Vision*, pages 622–631, 2019. 3
- [32] Kate Rakelly, Evan Shelhamer, Trevor Darrell, Alyosha Efros, and Sergey Levine. Conditional networks for few-shot semantic segmentation. *ICLR Workshop*, 2018. 3
- [33] Kate Rakelly, Evan Shelhamer, Trevor Darrell, Alexei A Efros, and Sergey Levine. Few-shot segmentation propagation with guided networks. *arXiv preprint arXiv:1806.07373*, 2018. 3
- [34] Shaoqing Ren, Kaiming He, Ross Girshick, and Jian Sun. Faster r-cnn: Towards real-time object detection with region proposal networks. In *Advances in neural information processing systems*, pages 91–99, 2015. 3, 6
- [35] Hamid Rezaatofighi, Nathan Tsoi, JunYoung Gwak, Amir Sadeghian, Ian Reid, and Silvio Savarese. Generalized intersection over union: A metric and a loss for bounding box regression. In *Proceedings of the IEEE Conference on Computer Vision and Pattern Recognition*, pages 658–666, 2019. 4
- [36] Amirreza Shaban, Shray Bansal, Zhen Liu, Irfan Essa, and Byron Boots. One-shot learning for semantic segmentation. In *Proceedings of the 28th British Machine Vision Conference (BMVC)*, 2017. 3
- [37] Mennatullah Siam, Boris Oreshkin, and Martin Jagersand. Adaptive masked proxies for few-shot segmentation. *arXiv preprint arXiv:1902.11123*, 2019. 3
- [38] Karen Simonyan and Andrew Zisserman. Very deep convolutional networks for large-scale image recognition. *arXiv preprint arXiv:1409.1556*, 2014. 3
- [39] Zhi Tian, Chunhua Shen, Hao Chen, and Tong He. Fcos: Fully convolutional one-stage object detection. In *Proceedings of the IEEE International Conference on Computer Vision*, pages 9627–9636, 2019. 2, 3, 6
- [40] Eduard Trulls, Stavros Tsogkas, Iasonas Kokkinos, Alberto Sanfeliu, and Francesc Moreno-Noguer. Segmentation-aware deformable part models. In *Proceedings of the IEEE Conference on Computer Vision and Pattern Recognition*, pages 168–175, 2014. 3
- [41] Kaixin Wang, Jun Hao Liew, Yingtian Zou, Daquan Zhou, and Jiashi Feng. Panet: Few-shot image semantic segmentation with prototype alignment. In *Proceedings of the IEEE International Conference on Computer Vision*, pages 9197–9206, 2019. 3
- [42] Yuxin Wu and Kaiming He. Group normalization. In *Proceedings of the European Conference on Computer Vision (ECCV)*, pages 3–19, 2018. 6
- [43] Xiaopeng Yan, Ziliang Chen, Anni Xu, Xiaoxi Wang, Xi-aodan Liang, and Liang Lin. Meta r-cnn : Towards general solver for instance-level low-shot learning. In *Proc. of IEEE International Conference on Computer Vision (ICCV)*, 2019. 1, 3, 4, 7, 8
- [44] Yuwei Yang, Fanman Meng, Hongliang Li, Qingbo Wu, Xiaolong Xu, and Shuai Chen. A new local transformation module for few-shot segmentation. In *International Conference on Multimedia Modeling*, pages 76–87. Springer, Cham, 2020. 3
- [45] Chi Zhang, Guosheng Lin, Fayao Liu, Jiushuang Guo, Qingyao Wu, and Rui Yao. Pyramid graph networks with connection attentions for region-based one-shot semantic segmentation. In *Proceedings of the IEEE International Conference on Computer Vision*, pages 9587–9595, 2019. 3
- [46] Chi Zhang, Guosheng Lin, Fayao Liu, Rui Yao, and Chunhua Shen. Canet: Class-agnostic segmentation networks with iterative refinement and attentive few-shot learning. In *Proceedings of the IEEE Conference on Computer Vision and Pattern Recognition*, pages 5217–5226, 2019. 3
- [47] Xiaolin Zhang, Yunchao Wei, Yi Yang, and Thomas Huang. Sg-one: Similarity guidance network for one-shot semantic segmentation. *arXiv preprint arXiv:1810.09091*, 2018. 3
- [48] Xingyi Zhou, Dequan Wang, and Philipp Krähenbühl. Objects as points. *arXiv preprint arXiv:1904.07850*, 2019. 3

Supplementary Material

1. Full COCO metrics of FAPIS: Tab. 6 and Tab. 7 show the average over five runs of full COCO metrics of FAPIS on object detection and instance segmentation respectively.

# shots	Part	AP	AP ₅₀	AP ₇₅	AP _S	AP _M	AP _L	AR ₁	AR ₁₀	AR ₁₀₀	AR _S	AR _M	AR _L
K=1	COCO-20 ⁰	12.8	20.9	13.2	8.7	13.9	18.8	11.9	28.1	38.8	24.0	41.7	51.9
	COCO-20 ¹	12.0	20.4	12.3	6.9	14.1	17.2	12.3	31.5	44.6	31.2	51.3	59.7
	COCO-20 ²	11.6	20.0	11.7	9.0	10.7	19.1	10.9	28.8	42.9	31.7	46.6	57.6
	COCO-20 ³	15.1	23.4	15.9	10.5	13.7	19.1	14.4	33.7	46.1	32.4	49.8	59.5
K=5	COCO-20 ⁰	14.1	22.6	14.6	8.3	14.8	22.0	13.2	28.9	39.4	24.5	41.9	54.0
	COCO-20 ¹	13.4	22.8	13.7	7.1	15.9	19.6	13.8	33.1	45.8	33.1	53.8	61.0
	COCO-20 ²	13.0	22.6	13.4	9.6	13.0	21.2	12.0	31.0	43.9	33.3	47.6	59.1
	COCO-20 ³	16.9	26.4	18.0	11.3	15.3	23.8	15.2	35.0	47.3	33.1	51.4	61.7

Table 6. Object detection results of FAPIS on full COCO metrics

# shots	Part	AP	AP ₅₀	AP ₇₅	AP _S	AP _M	AP _L	AR ₁	AR ₁₀	AR ₁₀₀	AR _S	AR _M	AR _L
K=1	COCO-20 ⁰	10.2	18.8	10.1	5.7	9.7	18.0	9.8	23.3	31.4	18.9	33.6	42.8
	COCO-20 ¹	8.9	17.7	8.0	3.8	10.4	15.7	10.1	26.0	36.7	23.0	44.2	50.6
	COCO-20 ²	9.8	18.2	9.7	4.3	8.9	18.3	10.5	24.8	35.9	26.2	39.6	48.7
	COCO-20 ³	12.5	21.4	13.3	7.1	11.4	19.2	12.6	28.3	37.4	22.9	41.4	52.8
K=5	COCO-20 ⁰	11.3	20.2	10.9	5.0	10.5	20.8	10.9	24.0	32.1	18.9	33.9	45.8
	COCO-20 ¹	10.3	20.0	9.4	3.8	11.9	19.0	11.2	27.6	38.4	24.4	46.0	54.7
	COCO-20 ²	11.4	20.4	12.1	6.5	10.6	20.4	11.3	25.5	35.5	24.4	39.3	47.9
	COCO-20 ³	14.3	24.3	15.0	7.5	13.3	22.9	13.5	30.1	39.6	24.8	43.8	54.3

Table 7. Instance segmentation results of FAPIS on full COCO metrics



Figure 6. Our one-shot instance segmentation on COCO-20¹.

2. Further qualitative results: We show more qualitative results on COCO-20ⁱ, $i = 1..3$ in Fig. 6, Fig. 7, Fig. 8, respectively. For each pair of images, the small one is the support and the large one is the query. Each instance segmentation

result is marked with a different color in the query. The green border indicates success cases, and the red border marks failure cases. FAPIS typically fails when instances in the support image are very different in appearance, shape, or 3D pose from instances in the query. Best viewed in color.



Figure 7. Our one-shot instance segmentation on COCO-20².



Figure 8. Our one-shot instance segmentation on COCO-20³.

3. Visualization of 16 latent parts: We show visualization of learned parts and their weights contributing to the final masks from COCO-20⁰ validation set in Fig. 9.

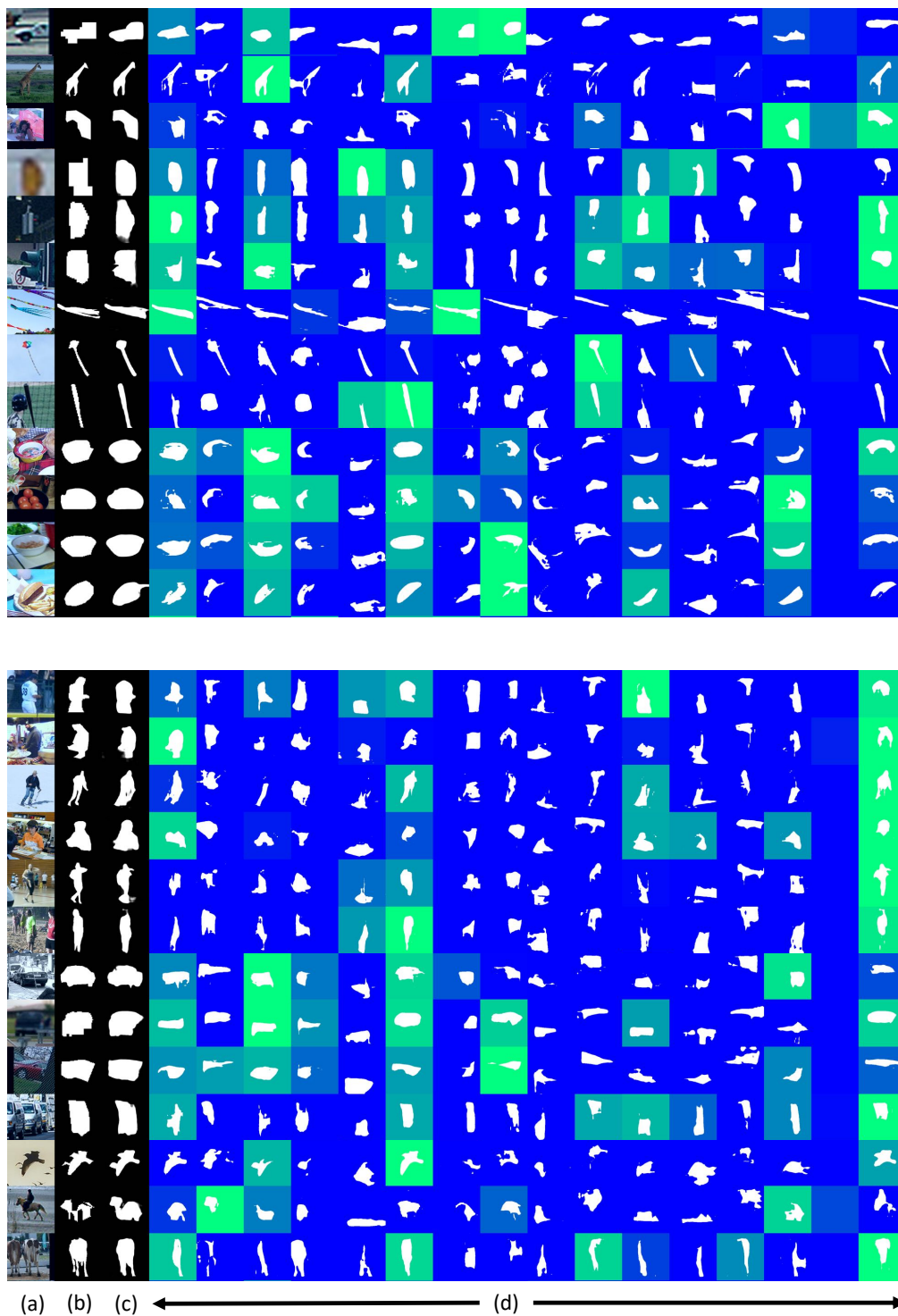


Figure 9. Visualization of 16 latent parts for both training (upper) and test (lower) classes from COCO-20⁰ validation set. From left to right: (a) input image, (b) GT segmentation, (c) predicted segmentation, (d) 16 predicted object parts. The predicted importance of the parts is color-coded from blue (smallest) to green (largest).